J|A|C|S ARTICLES

Published on Web 01/02/2009

Radiative Recombination of Spatially Extended Excitons in (ZnSe/CdS)/CdS Heterostructured Nanorods

Nishshanka N. Hewa-Kasakarage,[†,§] Maria Kirsanova,[†,§] Alexander Nemchinov,[†,§] Nickolas Schmall,[†,§] Patrick Z. El-Khoury,[‡,§] Alexander N. Tarnovsky,[‡,§] and Mikhail Zamkov*[,†,§]

The Center for Photochemical Sciences, Department of Physics, and Department of Chemistry, Bowling Green State University, Bowling Green, Ohio 43403

Received October 21, 2008; E-mail: zamkovm@bgsu.edu

Abstract: We report on organometallic synthesis of luminescent (ZnSe/CdS)/CdS semiconductor heterostructured nanorods (hetero-NRs) that produce an efficient spatial separation of carriers along the main axis of the structure (type II carrier localization). Nanorods were fabricated using a seeded-type approach by nucleating the growth of 20−100 nm CdS extensions at [000 ± 1] facets of wurtzite ZnSe/CdS core/shell nanocrystals. The difference in growth rates of CdS in each of the two directions ensures that the position of ZnSe/CdS seeds in the final structure is offset from the center of hetero-NRs, resulting in a spatially asymmetric distribution of carrier wave functions along the heterostructure. Present work demonstrates a number of unique properties of (ZnSe/CdS)/CdS hetero-NRs, including enhanced magnitude of quantum confined Stark effect and subnanosecond switching of absorption energies that can find practical applications in electroabsorption switches and ultrasensitive charge detectors.

1. Introduction

Synthesis of colloidal heterostructured nanocrystals (NCs) or nanorods (NRs) offers an effective route for the integration of multiple nanostructures with different functionalities into a single nanoscale object without the use of organic linkers, setting the basis for the development of a new generation of optoelectronic devices. Over the years, research on hetero-NCs has evolved from the synthesis of spherical core/shell quantum dots[1−9] to more complex shapes, including branched tetrapods,[10−12] barbells,[13−15] and hyper-branched heterostructures,[16,17] where the use of band-gap engineering has provided additional means to control the spatial distribution of charges across material junctions. Recently, a great deal of such synthetic work has been focused on the development of so-called type II hetero-NCs or NRs, constructed from two materials for which both the valance and conduction bands of one component lie lower in energy than the corresponding bands of the other component. The resulting staggered alignment of band edges at the material interface leads to spatial separation of the electron and hole in different parts of the heterostructure. In spatially asymmetric nanostructures, such separation of charges could be near complete, which gives rise to unique optical properties associated with an induced electric dipole. Potential areas of applicability for these materials include photovoltaic technologies, where spatially separated excitons require less energy for dissociation, anisotropic light sources, where an induced electric dipole allows achieving a high level of emission polarization, and optical modulators, where separation of carrier wave functions allows for switching of NC emission energies via quantum confined Stark effect.

Most of noncore/shell hetero-NCs that exhibit type II carrier localization regime have been based on the heterojunction of CdTe and CdSe semiconductors,[13−19] assembled using one of the two developed approaches, either by nucleating the growth

[†] Department of Physics.
[‡] Department of Chemistry.
[§] The Center for Photochemical Sciences.

(1) Kim, S.; Fisher, B.; Eisler, H. J.; Bawendi, M. *J. Am. Chem. Soc.* **2003**, *125*, 11466.
(2) Schöps, O.; Thomas, N. L.; Woggon, U.; Artemyev, M. V. *J. Phys. Chem. B* **2006**, *110*, 2074.
(3) Yu, K.; Zaman, B.; Romanova, S.; Wang, D.; Ripmeester, J. *Small* **2005**, *1*, 332.
(4) Xie, R.; Zhong, X.; Basché, T. *Adv. Mater.* **2005**, *17*, 2741.
(5) Cheng, C. T.; Chen, C. Y.; Lai, C. W.; Liu, W. H.; Pu, S. C.; Chou, P. T.; Chou, Y. H.; Chiu, H. T. *J. Mater. Chem.* **2005**, *15*, 3409.
(6) Danek, M.; Jensen, K. F.; Murray, C. B.; Bawendi, M. G. *Chem. Mater.* **1996**, *8*, 173.
(7) Ivanov, S. A.; Nanda, J.; Piryatinski, A.; Achermann, M.; Balet, L. P.; Bezel, I. V.; Anikeeva, P. O.; Tretiak, S.; Klimov, V. I. *J. Phys. Chem. B* **2004**, *108*, 10625.
(8) Ivanov, S. A.; Piryatinski, A.; Nanda, J.; Tretiak, S.; Zavadil, K. R.; Wallace, W. O.; Werder, D.; Klimov, V. I. *J. Am. Chem. Soc.* **2007**, *129*, 11708.
(9) Pandey, A.; Guyot-Sionnest, P. *J. Phys. Chem. B* **2007**, *127*, 104710.
(10) Talapin, D. V.; Nelson, J. H.; Shevchenko, E. V.; Aloni, S.; Sadtler, B.; Alivisatos, A. P. *Nano Lett.* **2007**, *7*, 2951.
(11) Carbone, L.; Kudera, S.; Carlino, E.; Parak, W. J.; Giannini, C.; Cingolani, R.; Manna, L. *J. Am. Chem. Soc.* **2006**, *128*, 748.
(12) Xie, R. G.; Kolb, U.; Basche, T. *Small* **2006**, *2*, 1454.
(13) Shieh, F.; Saunders, A. E.; Korgel, B. A. *J. Phys.Chem. B* **2005**, *119*, 8539.
(14) Halpert, J. E.; Porter, V. J.; Zimmer, J. P.; Bawendi, M. G. *J. Am. Chem. Soc.* **2006**, *128*, 12590.
(15) Kudera, S.; Carbone, L.; Casula, M. F.; Cingolani, R.; Falqui, A.; Snoeck, E.; Parak, W. J.; Manna, L. *Nano Lett.* **2005**, *5*, 445.
(16) Kanaras, A. G.; Sonnichsen, C.; Liu, L.; Alivisatos, A. P. *Nano Lett.* **2005**, *5*, 2164.
(17) Milliron, D. J.; Hughes, S. M.; Cui, Y.; Manna, L.; Li, J.; Wang, L.; Alivisatos, A. P. *Nature* **2004**, *430*, 190.
(18) Peng, P.; Milliron, D. J.; Hughes, S. M.; Johnson, J. C.; Alivisatos, A. P.; Saykally, R. J. *Nano Lett.* **2005**, *5*, 1809.

10.1021/ja8082895 CCC: $40.75

of spherical nanoparticles on one or both sides of the rod,[13−15] which yields linear structures, such as barbells, or by using spherical quantum dots with zinc blende structure to nucleate the growth of multiple extensions,[13,16−19] which leads to a branched architecture, such as tetrapods. While the use of spherical NCs as nucleation sites leads to formation of highly uniform hetoro-NCs and hetero-NRs, where the number of branches is controlled by an appropriate surfactant, synthesis of linear heterostructures, which makes use of highly reactive facets for nucleation of the secondary material often results in a wide distribution of different shapes. For instance, the difference in the number or type of dangling bonds between 001 and $00\bar{1}$ facets in wurtzite CdSe NRs used for seeding the growth of linear CdTe/CdSe/CdTe structures causes uncertainty in the nucleation event resulting in formation of either one- or two-sided barbells.[14] The presence of nonuniform shapes in a macroscopic volume of linear hetero-NRs lowers the degree of long-range order, complicating the controlled assembly of these structures onto a substrate via external fields[20−24] or through interparticle interactions.[25−27] Nonhomogeneous distribution of shapes and the absence of fluorescence (quantum yield < 1%) in CdTe/CdSe-based heterostructures hampered their utilization in optoelectronic devices, stressing the need for alternative directions in the synthesis of type II hetero-NRs.

Recently, a novel approach to synthesis of luminescent, type I CdSe/CdS hetero-NRs has been reported in the literature.[28] This method relies on small wurtzite CdSe NCs to nucleate the growth of CdS rods along the crystalline *c* axis and yields high-quality structures that are easily oriented in close-packed ordered arrays over large areas. The study also showed that the structural composition of original CdSe seeds was preserved during the synthesis, such that the emission of hetero-NRs was largely determined by the type I recombination of carriers in a CdSe/CdS heterojunction.

Here, we demonstrate that a general method of nucleating the growth of nanorods from spherical semiconductor NCs can be successfully adapted for the synthesis of hetero-NRs with type II carrier confinement. By using ZnSe/CdS core/shell NCs as nucleation sites for the growth of secondary CdS branches we fabricated homogeneously shaped (ZnSe/CdS)/CdS hetero-NRs exhibiting strong emission associated with type II relaxation of carriers across the ZnSe/CdS junction (see Figure 1). The location of the original ZnSe/CdS seed within the final structure is offset from its center by approximately 1/4−1/3 of the rod length, which results in a spatially asymmetric distribution of carrier wave functions along hetero-NRs. The linear separation

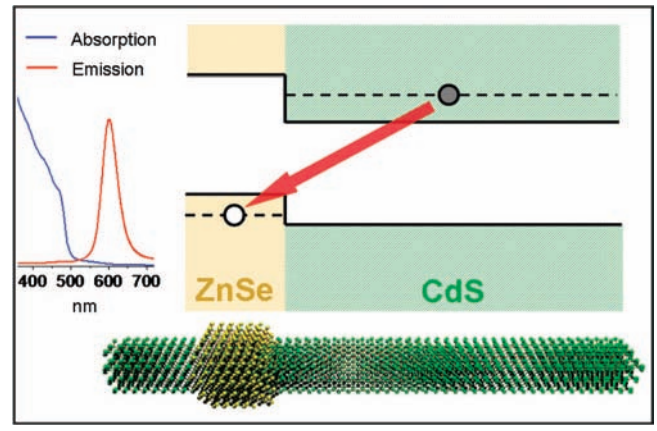

Figure 1. Spatial localization of photogenerated carriers in (ZnSe/CdS)/CdS hetero-NRs.

of carriers within such structural arrangement can be modulated with amplitudes of nearly one-half the rod's length, as inferred from the observed magnitude of the quantum confined Stark effect. Finally, shape control of (ZnSe/CdS)/CdS hetero-NRs can be realized in a straightforward manner by varying concentrations of Cd and S precursors during the final stage of synthesis. Indeed, high concentrations of injection precursors lead to formation of pill-like structures, where the seed was fully incorporated within the body of hetero-NRs, while use of dilute Cd and S stock solutions promoted the growth of high-aspect-ratio NRs, where the initial nucleation of CdS occurred on one of the facets of the seeding particle, such that the center of the seed was offset from the central axis of CdS rod by as much as 2 nm. An offset of band edges at the interface of ZnSe and CdS materials promotes spatial separation of an electron−hole pair into opposite parts of the structure such that an electron wave function becomes primarily localized within CdS and a hole within ZnSe semiconductor materials. The subsequent recombination of spatially separated excitons occurs across the ZnSe/CdS interface, leading to a considerable red shift of the emission peak in (ZnSe/CdS)/CdS hetero-NRs, with respect to the absorption edge in ZnSe (420 nm) and CdS (440 nm) NCs, as evident from the insert plot showing absorption and emission spectra of hetero-NRs.

The seeded-type approach to the synthesis of type II hetero-NRs provides an effective way to fabricate regularly shaped heterostructures with a narrow distribution of lengths. In contrast to type II NRs based on a CdTe/CdSe heterojunction of materials, (ZnSe/CdS)/CdS hetero-NRs, reported here, are strongly luminescent, which allows for their utilization in both photovoltaic and light-emitting applications.

2. Experimental Section

2.1. Chemicals. Cadmium oxide (99%, Aldrich), sulfur (99.9%, Aldrich), zinc stearate (99%, Across), 1-octadecene (ODE, 90%, Aldrich), tributylphosphine (TBP, 99%, Aldrich), oleic acid (OA, 90%, Aldrich), trioctylphosphine (TOP, 97%, Strem) trioctylphosphine oxide (TOPO, 99%, Aldrich), hexadecylamine (HPA, 99%, Aldrich), octadecylamine (ODA, 99%, Aldrich), *n*-octadecylphosphonic acid (ODPA, 99%, Polycarbon), anhydrous hexane (Aldrich), methanol (Aldrich), chloroform (Acros), and toluene (Aldrich) were used as purchased.

All reactions were conducted under argon using standard Schlenk techniques.

2.2. Synthesis of ZnSe Seeds. Synthesis of monodisperse wurtzite ZnSe nanocrystals was based on a procedure described in

(19) Li, Y. C.; Zhong, H. Z.; Li, R.; Zhou, Y.; Yang, C. H.; Li, Y. F. *Adv. Funct. Mater.* **2006**, *16*, 1705.
(20) Harnack, O.; Pacholski, C.; Weller, H.; Yasuda, A.; Wessels, J. M. *Nano Lett.* **2003**, *3*, 1097.
(21) Ryan, K. M.; Mastroianni, A.; Stancil, K. A.; Liu, H. T.; Alivisatos, P. *Nano Lett.* **2006**, *6*, 1479.
(22) Gupta, S.; Zhang, Q.; Emrick, T.; Russell, T. P. *Nano Lett.* **2006**, *6*, 2066.
(23) Hu, Z.; Fischbein, M. D.; Querner, C.; Drndic′, M. *Nano Lett* **2006**, *6*, 2585.
(24) Nobile, C.; Fonoberov, V. A.; Kudera, S.; Torre, A. D.; Ruffino, A.; Chilla, G.; Kipp, T.; Heitmann, D.; Manna, L.; Cingolani, R.; Balandin, A. A.; Krahne, R. *Nano Lett.* **2007**, *7*, 476.
(25) Li, L. S.; Walda, J.; Manna, L.; Alivisatos, A. P. *Nano Lett.* **2002**, *2*, 557.
(26) Dumestre, F.; Chaudret, B.; Amiens, C.; Respaud, M.; Fejes, P.; Renaud, P.; Zurcher, P. *Angew. Chem., Int. Ed.* **2003**, *42*, 5213.
(27) Talapin, D. V.; Shevchenko, E. V.; Murray, C. B.; Kornowski, A.; Forster, S.; Weller, H. *J. Am. Chem. Soc.* **2004**, *126*, 12984.
(28) Carbone, L. *Nano Lett.* **2007**, *7*, 2942.

ref 29 as follows. A 0.3794 g (0.6 mmol) amount of zinc stearate was dissolved in 9.5 mL (3.2 g) of octadecane by heating reagents to 300 °C in the 25 mL three-neck flask while stirring. After the mixture became clear, selenium stock solution, prepared by dissolving 0.0474 g (0.6 mmol) of selenium in 1.5 mL of TOP, was swiftly injected into the reaction flask. During the nanocrystal growth, the temperature was kept at 290 °C. The reaction was stopped after 13 min by removing the flask from the heating mantle. After the reaction mixture was allowed to cool to 50 °C, 3−5 mL of hexane was added into the solution to prevent solidification. Subsequent cleaning of nanocrystals was done by hexane/methanol extraction. Typically 6−7 mL of methanol was added to the reaction mixture in hexane, which was then centrifuged for 10 min at 3500 rpm. The upper hexane layer containing QDs was taken with a syringe for further purification. The final clear suspension was then placed under argon and stored in the dark for future shell deposition.

2.3. Synthesis of Small ZnSe/CdS Core/Shell NCs. In the next step, purified and size-selected ZnSe NCs were then overcoated with 1−2 monolayers of CdS using a previously developed procedure.[30] For shell deposition injection stock solutions were prepared at a concentration of 0.04 M in ODE. Cadmium was obtained by dissolving 0.030 g (0.24 mmol) of cadmium oxide in 0.6 mL of OA and 5.4 mL of ODE in a 25 mL flask under argon by heating it to 280 °C while stirring. After the solution became clear it was cooled to 60 °C. The sulfur injection solution was prepared from 0.0077 g (0.24 mmol) of sulfur dissolved in 6 mL of ODE by heating the mixture to 200 °C under argon flow. For continuous shell deposition both precursors were mixed together and injected into the reaction vessel containing previously prepared ZnSe nanocrystals dispersed in 1.5 g of ODA and 6.3 mL of ODE at 240 °C. The injection rate was 2 mL/h. Aliquots of the reaction mixture were taken at 7−10 min intervals for UV−vis and PL spectral characterization.

2.4. Synthesis of (ZnSe/CdS)/CdS Hetero-NRs. Growth of CdS extensions from ZnSe/CdS seeds was done using a technique adapted from ref 28. The cadmium injection solution was prepared by combining 0.060 g (0.47 mmol) of cadmium oxide, 3 g of TOPO, 0.290 g of ODPA, and 0.080 g of hexadecylamine (HPA) in a 25 mL three-neck flask. The mixture was then pumped at 150 °C for 30 min to remove air, switched to argon, and heated to 380 °C while stirring. After the solution became clear, 1.81 mL of TOP was injected and the temperature was recovered to 380 °C.

The sulfur solution was prepared by dissolving 0.120 g (3.74 mmol) of sulfur in 1.81 mL of TOP at 180 °C under argon flow. After cooling to 60 °C, the sulfur solution was combined with 3−8 mL of ZnSe/CdS NC solution in TOP (the increase in the amount of TOP corresponds to the increase in the aspect ratio of final heterorods). The concentration of seed NCs was chosen so that the product of the absorbance at 500 nm and suspension volume was in the range of 30−40 mL. The mixture was stirred for 10 min and injected into the reaction flask. The temperature was recovered to 390 °C in 3 min, and the growth phase took 7−10 min. The reaction mixture was let to cool to 60 °C and purified using hexane/methanol extraction.

2.5. Characterization. UV−vis absorption and photoluminescence (PL) spectra were recorded using a CARY 50 Scan spectrophotometer and Jobin Yvon Fluorolog FL3-11 fluorescence spectrophotometer. PL quantum yield of hetero-NCs was determined relative to known QYs of several organic dyes excited at 400−440 nm. High-resolution transmission electron microscopy measurements were carried out using a JEOL 311UHR operated at 300 kV. Specimens were prepared by depositing a drop of nanocrystal hexane solution onto a Formvar-coated copper grid and letting it dry in air. X-ray powder diffraction measurements were carried out on Scintag XDS-2000 X-Ray Powder Diffractometer. Energy-dispersive X-ray (EDX) emission spectra were measured using an EDAX X-ray detector located inside a scanning electron microscope. The electron beam was accelerated at 20 kV. Picosecond transient absorption measurements were performed using a home-built laser system comprising a Ti:Sapphire regenerative amplifier and TOPAS-C optical parametric amplifier operating at 1 kHz. Instrument response time was estimated to be less than 1 ps.

3. Results and Discussion

Synthesis of (ZnSe/CdS)/CdS NRs is performed at temperatures that exceed the threshold for homogeneous nucleation, allowing for both homogeneous and heterogeneous growth mechanisms to contribute to formation of nanorods. When the concentration of precursors is low, nucleation of CdS occurs primarily at high reactivity facets [000±1] of ZnSe/CdS seed nanoparticles, such that growth of CdS rods is mostly heterogeneous.[31] For high concentrations of precursors, the activation energy for homogeneous nucleation becomes lower and an appreciable isotropic growth occurs. In this work, the competition between homogeneous and heterogeneous nucleation processes is controlled by varying the amount of TOP in the injection solution, such that injections with higher concentrations of precursors yield a lesser fraction of homogeneous nucleation and vice versa.

High-aspect-ratio hetero-NRs, fabricated using low concentrations of precursors (Cd- and S-limited conditions) are shown in Figure 2a−d. An outline of the original ZnSe/CdS seed can be distinguished in most of the fabricated hetero-NRs, while its presence within the rod structure is confirmed by energy-dispersive X-ray measurements (Figure 2i) that show traces of both Zn and Se elements. The location of the seed appears to be offset from the center of the heterostructure by approximately 1/4−1/3 of the rod's length. The average seed diameter in the final structure is just slightly greater than the size of core/shell NCs prior to synthesis of CdS extensions, which indicates that NC growth occurs predominantly via heterogeneous nucleation. The two images shown in Figure 2c and 2d reveal that in addition to an asymmetric placement of ZnSe/CdS NCs along the nanorod axis some of the seeds may also exhibit a lateral shift, such that the center of ZnSe/CdS NC is offset from the main axis of the rod by as much as 2 nm. A cause of this structural effect can be seen in the high-resolution TEM images, showing that the direction of nanorod growth is not always parallel to the *c* axis of ZnSe/CdS seeds, such that the center of the seeding NCs is shifted from the 00±1 nucleation cite. By examining 35 specimens under 300 000× magnification we determined the average length of high-aspect-ratio hetero-NRs, such as the ones shown in Figure 2a−d, to be 106 nm (Figure 3a). The standard deviation of length distribution was 13.2 nm or 12%.

CdS hetero-NRs fabricated with high concentrations of precursors are shown in Figure 2e−h. Most of the structures exhibit symmetric pill-like shapes with an average aspect ratio of 2.5. High-magnification analysis (Figure 2h) reveals that original ZnSe/CdS seeds are fully incorporated within the nanoparticle body, indicating that significant homogeneous growth occurs during the synthesis, leading to an isotropic enhancement of hetero-NRs in the direction perpendicular to the crystalline *c* axis. Despite a mixed growth mechanism the length distribution of pill-like structures (10%) was found to be lower than that of high-aspect-ratio hetero-NRs.

(29) Reiss, P.; Quemard, G.; Carayon, S.; Bleuse, J.; Chandezon, F.; Pron, A. *Chem. Mater.* **2004**, *84*, 10.
(30) Nemchinov, A.; Kirsanova, M.; Hewa-Kasakarage, N. N.; Zamkov, M. *J. Phys. Chem. C* **2008**, *112*, 9301.
(31) Mokari, T.; Rothenberg, E.; Popov, I.; Costi, R.; Banin, U. *Science* **2004**, *304*, 1787.

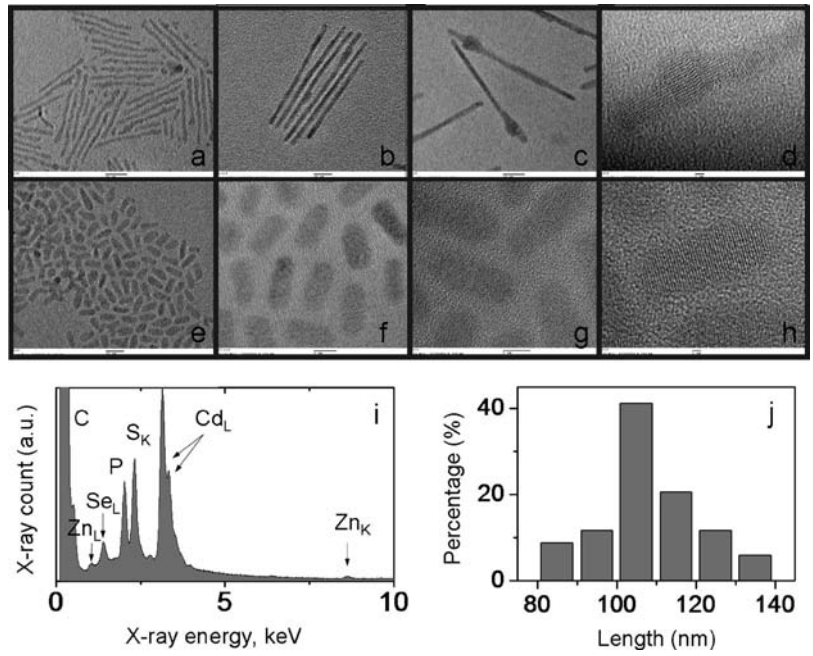

Figure 2. Transmission electron microscope images of (ZnSe/CdS)/CdS hetero-NRs fabricated using low (a−d) and high (e−h) concentrations of precursors. The location of ZnSe/CdS seeds within high-aspect-ratio hetero-NRs can be distinguished in c and d. Scale bars are as follows: (a−c, e) 20 nm, (f and g) 5 nm, (d and h) 1 nm. (i). Energy-dispersive X-ray spectrum of high-aspect-ratio (ZnSe/CdS)/CdS hetero-NRs. (j) Length distribution of high-aspect-ratio (ZnSe/CdS)/CdS hetero-NRs.

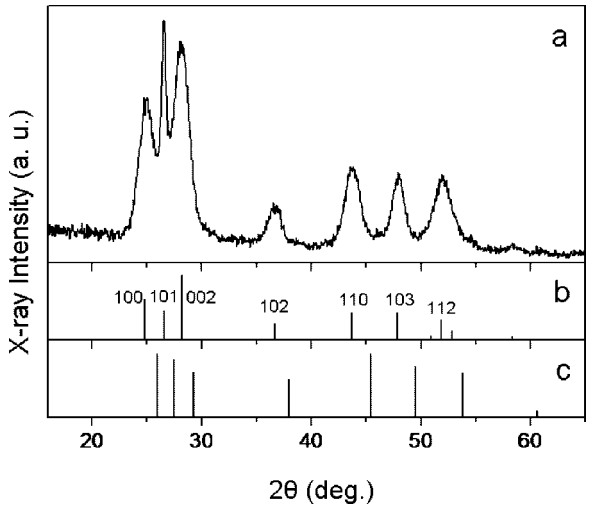

Figure 3. (a). X-ray powder diffraction spectra of (ZnSe/CdS)/CdS hetero-NRs along with diffraction patterns of bulk wurtzite CdS (b) and ZnSe (c).

X-ray powder diffraction (XPD) measurements were performed to verify the wurtzite lattice structure of fabricated materials. The experimental diffraction pattern, obtained for high-aspect-ratio (ZnSe/CdS)/CdS hetero-NRs, is shown in Figure 3b. As evident from comparison of diffraction patterns for bulk wurtzite CdS (Figure 3c) and ZnSe (Figure 3d) lattices the observed set of Bragg peaks corresponds to the wurtzite phase of CdS. The absence of XPD signal from ZnSe lattice is consistent with a prevailing amount of CdS material in the final hetero-NR structure (approximately 97% by volume) as well as with the core/shell arrangement of ZnSe/CdS NCs[30] that enhances the XPD intensity of the shell material.

Figure 4 summarizes optical properties of nanostructures obtained after each of the three fabrication stages involved in the synthesis of (ZnSe/CdS)/CdS hetero-NRs. Spectral characteristics of ZnSe NCs fabricated in the first step (Figure 4a) are consistent with typical features of monodisperse binary NCs exhibiting a sharp absorption edge and a narrow emission bandwidth. A small amount of trap state emission, distinguishable in FL spectra as a broad, structureless, tail, centered at 490 nm (see Figure 4d, spectrum 1), is caused by interaction of the solvent with the surface of ZnSe NCs, which is passivated only by organic ligands. The contribution of these trap states to the emission in ZnSe NCs becomes particularly evident when the capping layer of TOP is thermally perturbed at the beginning of the second fabrication stage, as seen in spectrum 2 of Figure 4d. Here, these traps are referred to as deep due to the core localization of these states in the layered hetero-NR assembly.

Deposition of a thin CdS shell onto ZnSe NCs results in the development of a low-energy tail in the absorption profile (Figure 4b), which extends over the visible range due to an onset of type II localization regime. This process is accompanied by quenching of type I violet emission in ZnSe NCs and the appearance of the new emission feature in the visible range. Deep trap FL associated with the original ZnSe cores can be still observed around 490 nm, as seen in Figure 4d, spectrum 3; however, it does not match the emission peak at 540 nm corresponding to carrier recombination in type II ZnSe/CdS NCs. This excludes the possibility that deposition of the shell simply quenches the band edge FL of ZnSe NCs while the deep trap emission remains. The longer FL lifetime of ZnSe/CdS core/shell NCs relative to that of binary ZnSe NCs (Figure 4e) serves as additional evidence that the contribution of deep traps in ZnSe is reduced upon deposition of CdS shell. According to the emission profile in Figure 4d, spectrum 3, formation of the ZnSe/CdS interface gives rise to another type of trap states, whose emission is red shifted from the position of the spatially indirect FL ($1S_e(CdS)-1S_h(ZnSe)$) in core/shell NCs. The intensity of this emission peak is gradually reduced with the increasing thickness of CdS shell, indicating that its origin is likely to be related to electron or holes traps at the ZnSe/CdS interface rather

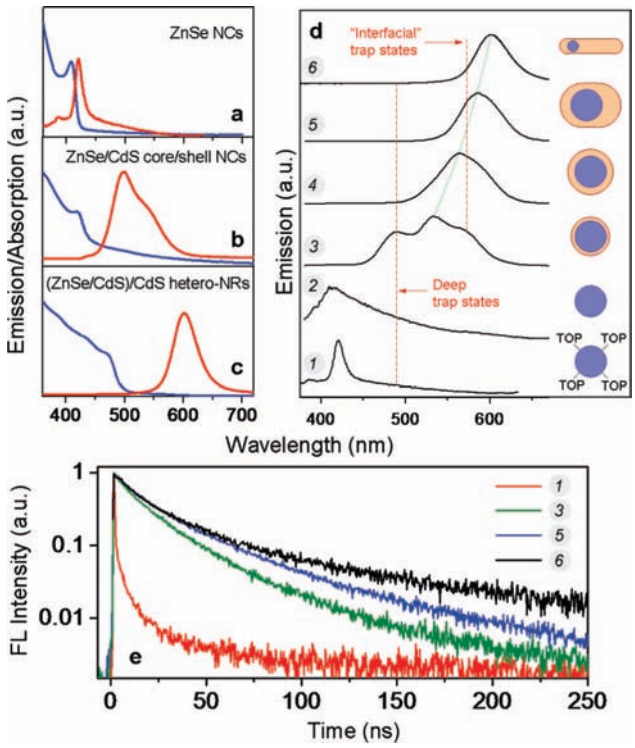

Figure 4. Optical characteristics of NC and NR colloids. UV−vis absorption and steady-state fluorescence spectra for: (a) 5 nm diameter ZnSe NCs, (b) ZnSe/CdS core/shell NCs, fabricated by depositing 2−3 monolayers of CdS, and (c) high-aspect ratio (ZnSe/CdS)/CdS hetero-NRs. (d) Evolution of the FL spectra during the three-stage synthesis, showing the trap state emission. Deep traps contribute to the emission near 490 nm as evidenced by the broad emission tail in passivated (spectrum 1) and unpassivated (spectrum 2) ZnSe NCs. ZnSe/CdS core/shell NCs with ca. 1 monolayer of CdS exhibit both deep and interfacial trap emission (spectrum 3). The former becomes quenched in thick-shell ZnSe/CdS NCs (spectrum 4), while the latter is reduced in large-size (oblong) core/shell structures (spectrum 5) and becomes fully quenched in long (ZnSe/CdS)/CdS hetero-NRs (spectrum 6). (e). FL intensity decay for ZnSe (red), thin-shell ZnSe/CdS NCs (green), thick-shell ZnSe/CdS NCs (blue), and (ZnSe/CdS)/CdS hetero-NRs (black), measured by means of TCSPC technique.

than dangling bonds on the surface of CdS. Growth of short, 1−2 nm CdS extensions at the final stage of the synthesis leads to a near complete quenching of both deep and interfacial trap emissions as well as further red shifting of the spatially indirect FL, as shown in the spectrum 5 of Figure 4d. The diminishing contribution of traps to carrier relaxation for these structures is also evidenced by the increasing lifetime of the FL intensity decay (Figure 4e, blue curve).

Optical characteristics of high-aspect-ratio (ZnSe/CdS)/CdS hetero-NRs are shown in Figure 4c. Due to the delocalization of electronic wave functions over the increased volume of CdS the emission of 106 nm hetero-NRs undergoes a 10−15 nm red shift from the peak position in short-branched (ZnSe/CdS)/CdS heterostructures (spectrum 5 in Figure 4d). Growth of linear CdS extensions is also accompanied by the 10−20 nm decrease in the spectral width of the emission, which is consistent with further quenching of trap state emission as well as the increase of CdS shell beyond the "saturation" value associated with the onset of type II localization regime.[30] The FL quantum yield (QY) of as-prepared high-aspect-ratio hetero-NRs diluted in chloroform was typically in the range of 8−18% and further improved to 14−25% after purification by hexane-50% + chloroform-50%/methanol extraction.

The FL intensity decay of 106 nm (ZnSe/CdS)/CdS hetero-NRs is shown by a black curve in Figure 4e. It is expected that radiative relaxation of spatially separated excitons may exhibit unique relaxation times that arise from intrinsically different carrier decay mechanisms associated with a weak-confinement regime. Owing to a nonzero quantum yield and spatial separation of charges, fabricated hetero-NRs provide a model system for testing such hypothesis. According to traces 5 and 6 in Figure 4e both short- and long-branched NRs exhibit nonexponential radiative relaxation of excited carriers, which is generally anticipated of semiconductor quantum systems due to mixing of contributions from different single-exponential lifetimes corresponding to "on" and "off" blinking cycles.[32] The FL lifetime of high-aspect-ratio hetero-NRs appears to be longer than in short-branched heterostructures (blue curve), which could be the result of fewer carrier traps present at the ZnSe/CdS interface or smaller overlap between electron and hole wave functions brought by delocalization of electrons in CdS. The overall character of carrier relaxation in high-aspect-ratio hetero-NRs, however, appears to be similar to that of short hetero-NRs or even core/shell NCs, indicating that a mechanism of radiative recombination across the ZnSe/CdS heterojunction is majorly independent of the degree of charge separation.

The dynamics of optical excitations in (ZnSe/CdS)/CdS hetero-NRs was further investigated using time-resolved transient absorption spectroscopy. This technique relies on measurements of excitation-induced changes in the absorption spectra (ΔA) and provides information on the relative population of excited states in the system. By using 1 ps of minimal delay between excitation and probe pulses we ensure that most carriers occupying high-energy states (nS, nP,..., $n > 1$) relax to band edges[33,34] such that the primary contribution to the bleaching signal comes from 1S(e,h) states. Figure 5a shows temporal changes in the absorption of hexane-suspended hetero-NRs excited with 420 nm monochromatic light. The spectrum contains three main areas of bleaching corresponding to spectral markers at 461, 482, and 557 nm. By comparing bleach positions with the absorption spectrum of hetero-NRs (Figure 4c) we were able to classify the origin of the observed intervals of bleaching at 461 and 557 nm as due to 1S(e)−1S(h) transitions in the CdS shell and ZnSe/CdS heterojunction, respectively. Meanwhile, the origin of the smaller signal at 482 nm was attributed to excitations of carriers in branch portions of hetero-NRs, where spatial delocalization of electronic wave functions results in a shift of the CdS absorption edge below the energy of the 1S(e)−1S(h) transition in the CdS shell. Similarities in the character of 461 and 482 nm excitations residing within the same semiconductor material are evidenced by the proximity of corresponding bleach recovery times, as shown in Figure 5c. Both relaxation trends exhibit an apparent correlation in the initial fast decay slopes as well as in the following slower bleach recovery time dependences.

A unique type of bleach recovery was observed for the 557 nm signal, corresponding to $1S_e(CdS)-1S_h(ZnSe)$ excitations in (ZnSe/CdS)/CdS hetero-NRs. As seen in the insert of Figure 5a, the spectral position of the ΔA minimum gradually red shifts from 552 to 590 nm over the period of

(32) Fisher, B. R.; Eisler, H. J.; Stott, N. E.; Bawendi, M. G *J. Phys. Chem. B* **2004**, *108*, 143.
(33) Puls, J; Jungnickel, V; Henneberger, F; Schulzgen, A. *J. Cryst. Growth* **1994**, *138*, 1004.
(34) Roberti, T. W; Cherepy, N. J; Zhang, J. Z. *J. Phys. Chem.* **1998**, *108*, 2143.

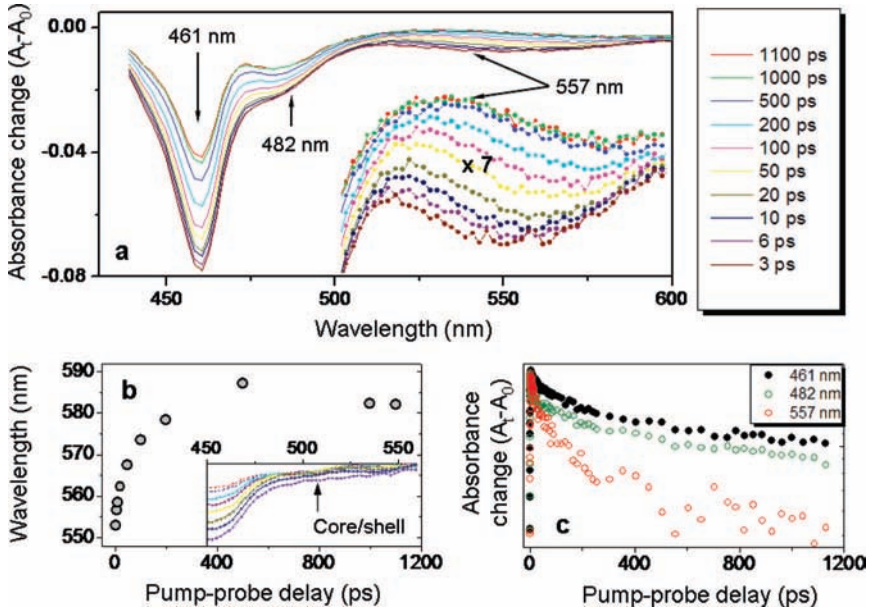

Figure 5. Measurements of the state-filling dynamics in (ZnSe/CdS)/CdS hetero-NRs performed with picosecond transient absorption. (a) Absorbance changes (ΔA) of hexane-suspended nanorods excited with 420 nm monochromatic light. Three main areas of photobleaching, corresponding to spectral markers at 461, 482, and 557 nm, were indentified. The insert provides a more detailed representation of absorbance changes in the 557 nm region showing time-dependent shifting of the 557 nm peak toward longer wavelengths. (b) Temporal evolution of the spectral position for the 557 nm bleach is shown. The insert shows the temporal evolution of ΔA for ZnSe/CdS core/shell NCs. (c) Bleach recovery dynamics for the three areas of photobleaching (461, 482, and 557 nm).

300 ps. This process is sufficiently slow for high-energy carriers to decay to the bottom of the band,[35,36] indicating that the change in the energy of the bleaching signal cannot be associated with either $2S_{3/2}(h)-1S_{3/2}(h)$ or $1P(e)-1S(e)$ carrier relaxation pathways. The observed shift of the ΔA minimum, on the other hand, can be linked to the decrease in the spatial confinement of electronic wave functions associated with a charge-separated state in (ZnSe/CdS)/CdS hetero-NRs. Indeed, the energy of e−h interaction in NCs is inversely proportional to the square of the confinement length, a, such that $\Delta E = -(h^2/8m_r a^2)$, where $m_r = (m_e^{-1} + m_h^{-1})^{-1}$. If we assume that an electron−hole pair is brought to a separation of 1/3 of the rod length (approximately 10 nm) from its initial confinement within ZnSe/CdS core/shell NCs ($a \approx 2.5$ nm) then the associated decrease in the energy of the 1S(e)−1S(h) transition, ΔE ($t = 1100$ ps) to ΔE ($t = 0$), will be 0.14 eV, which corresponds to a 37 nm red shift of the emission. This value is consistent with the 38 nm red shift observed in TA measurements (Figure 5a and 5b). The assumption that carriers are initially confined within the spherical core/shell NC is consistent with the larger amplitude of the bleaching signal originating from the CdS shell (461 nm) in comparison with the signal forming in the branch portion of hetero-NRs (482 nm). Additional support of the proposed delocalization-induced shift in the 557 nm signal is provided by the TA dynamics of ZnSe/CdS seeds (see the insert in Figure 5b) that confirms the absence of the spectral shift of the ZnSe/CdS bleach (denoted by an arrow) when excitons are restricted to a small volume of core/shell NCs. The temporal dynamics of the charge separation process is shown in Figure 5b, where the change in the position of the bleaching signal is plotted versus the pump−probe delay. By fitting the initial evolution of the wavelength with a single exponent we obtain the characteristic time scale for the separation process to be 54 ps.

The effect of external electric field on energy levels in a semiconductor heterostructure can be dramatically enhanced by the quantum confinement of carrier wave functions, causing sizable modulation of the position and width of the emission peak. This phenomenon, also known as quantum confined Stark effect (QCSE), has been demonstrated to produce detectable spectral changes in single, type II CdSe/CdS hetero-NRs, where an efficient red shifting of the emission peak was possible due to a sizable spatial separation of charges.[37,38] The value of the type II energy offset in (ZnSe/CdS)/CdS hetero-NRs exceeds that of CdSe/CdS combination of materials, which should produce a more complete separation of charges and thus more extensive QCSE-induced spectral changes.

To study the effect of electric field on the emission properties of (ZnSe/CdS)/CdS hetero-NRs a dilute nanorod suspension in hexane was injected into a sealed cuvette comprising two conducting windows separated by 40 μm. A direct voltage in the range from −120 to 120 V was then applied to the inner walls of the cuvette, creating electric fields of up to 30 kV/cm. The potential difference across (ZnSe/CdS)/CdS hetero-NRs, whose axes are parallel to the direction of the field, is determined as

$$\Delta V \approx Ed(\varepsilon_{\text{hexane}}/\varepsilon_{\text{rod}}) \qquad (1)$$

where E is the electric field, d is the nanorod's length, and $\varepsilon_{\text{hexane}} = 2.0$ and $\varepsilon_{\text{rod}} = 9.5$ are dielectric constants of the surrounding matrix and hetero-NRs, respectively. According to this equation

(35) Klimov, V. I.; Schwarz, C. J.; McBranch, D. W.; Leatherdale, C. A.; Bawendi, M. G. *Phys. Rev. B* **1999**, *60*, R2177.
(36) Klimov, V. I.; McBranch, D. W. *Phys. Rev. Lett.* **1998**, *80*, 4028.
(37) Mu1ller, J.; Lupton, J. M.; Lagoudakis, P. G.; Schindler, F.; Koeppe, R.; Rogach, A. L.; Talapin, D. V.; Weller, H.; Feldmann, J. *Nano Lett.* **2005**, *5*, 2044.
(38) Kraus, R. M.; Lagoudakis, P. G.; Rogach, A. L.; Talapin, D. V.; Weller, H.; Lupton, M.; Feldmann, J. *Phys. Rev. Lett.* **2007**, *98*, 017401.

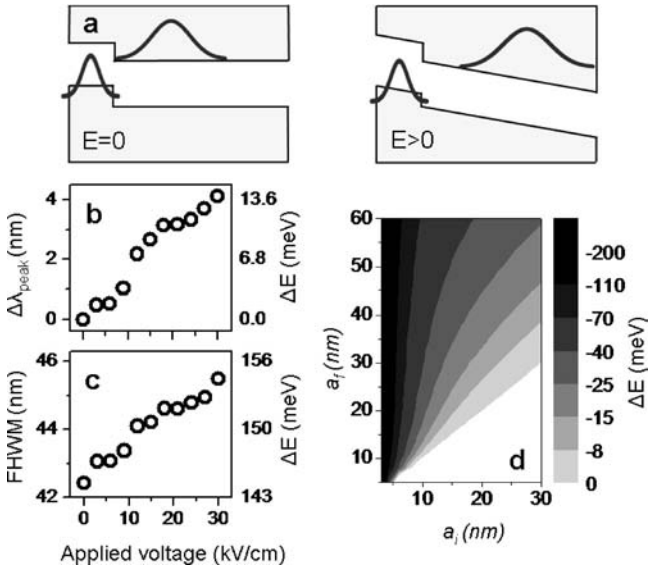

Figure 6. Quantum confined Stark effect in (ZnSe/CdS)/CdS hetero-NRs. (a) Schematic representation of field-induced changes in the nanocrystal potential and carrier localization pattern. (b) Observed red shifting, $\Delta\lambda$, of the FL peak in colloidal (ZnSe/CdS)/CdS hetero-NRs caused by external electric field. (c) Effect of electric field on the spectral width of the emission. (d) Expected amplitudes of the Stark shift for different sets of the initial (a_i) and final (a_f) electron−hole separation in (ZnSe/CdS)/CdS hetero-NRs.

the potential difference across a 100 nm hetero-NR, oriented along the field, is 0.06 V. The corresponding magnitude of the Stark shift is determined by the change in the electron−hole interaction energy, $\Delta E_{e\text{-}h}$, associated with the increased charge separation and the change of the electric potential energy along the NR axis ΔE_V

$$\Delta E_{Stark} = \Delta E_{e-h} + \Delta E_V = \left(\frac{h^2}{8m_r}\right)\left(\frac{1}{a_f^2} - \frac{1}{a_i^2}\right) - E(a_f - a_i)\left(\varepsilon_{matrix}/\varepsilon_{rod}\right) \quad (2)$$

where a_i and a_f are the initial and the final electron−hole separations in hetero-NRs, respectively.

The contour plot in Figure 6d shows expected values of ΔE_{Stark} for a NR oriented parallel to 30 kV/cm electric field, while Figure 6b shows the observed spectral changes in the emission of (ZnSe/CdS)/CdS hetero-NRs when the electric field is increased from 0 to 30 kV/cm. As expected, the position of the FL peak red shifts with an increasing voltage, reaching a maximum offset of 4.0 nm. The observed modulation of the emission wavelength is considerably larger than previously reported values for CdS/CdSe nanorods,[35] which is expected due to a greater type II band gap offset at the interface of ZnSe and CdS materials that creates a stronger confinement of the hole wave function on one side of the structure. The distribution of nanorod orientations is believed to be responsible for the field-induced inhomogeneous broadening of the emission peak, as shown in Figure 6c, caused by contributions from hetero-NRs aligned perpendicular to the field, whose emission is not affected by the applied voltage, and hetero-NRs oriented along the field, which emission undergoes a red shift in excess of 4 nm.

4. Conclusions

The present synthesis demonstrates a number of potential benefits associated with the use of ZnSe/CdS heterojunction for development of type II heterostructured nanorods. First, the large offset of band edges between ZnSe and CdS semiconductors promotes a more complete spatial separation of photogenerated carriers than can be expected from heterostructures utilizing CdSe/CdTe combination of materials. Second, the observation of strong, spatially indirect, emission in (ZnSe/CdS)/CdS hetero-NRs indicates that a significant portion of charge-separated states in ZnSe/CdS-based heterostructures can recombine radiatively, which has not been observed previously in other type II noncore/shell semiconductor nanomaterials. Finally, a combination of an efficient charge separation and excellent emissive properties in (ZnSe/CdS)/CdS hetero-NRs enhances the magnitude of a quantum confined Stark effect such that application of even small electric fields can produce detectable spectral modulations of the emission.

Acknowledgment. We gratefully acknowledge Bowling Green State University for financial support (SF07, RIC2008, RCE2008). This research made use of the facilities of the University of Michigan Electron Microbeam Analysis Laboratory and University of Toledo Instrumentation Center.

Note Added after ASAP Publication. While this article was in production, the authors learned about a similar work on ZnSe/CdS heterostructures performed by the group of Prof. U. Banin. Their paper is now cited as ref 39 (citation added January 7, 2009).

Supporting Information Available: Full author list for the ref 28 is provided. This material is available free of charge via the Internet at http://pubs.acs.org.

JA8082895

(39) Dorfs, D.; Salant, A.; Popov, I.; Banin, U. *Small* **2008**, *4*, 1319.